Impact factor: 2019: 4.679 2020: 5.015 2021: 5.436, 2022: 5.242, 2023:

6.995, 2024 7.75

#### WEAR RESISTANCE OF CUTTING TOOLS COATED FROM HEAT-RESISTANT, CHROME ALLOYS

**SHARIPOV J.O.** 

Asian International University

**ABSTRACT:** In this article, a comprehensive study of the effect of surface treatment with lowenergy electron beams on the structural and phase composition of the surface layer of a highspeed cutting tool, as well as on the microhardness and wear resistance of disk cutters, was carried out. The surfaces of high-speed tools made of R6M5 alloys, heat treated with nitriding, coated with a layer of NbHf alloy deposited by magnetron sputtering, are modified by electron beam processing. As a result, an interlayer is formed with the concentration of alloying elements, which gradually varies in depth. The results of the study of this composite using X-ray diffraction analysis are presented.

**Key words:** high-speed cutting tool, electron-beam processing, combined surface treatment.

**Introduction.** Increased requirements are imposed on the wear resistance of the surface of all modern tools. It is generally accepted to create on the surface of a tool a layer whose structure and chemical composition differ from its core. The most commonly used methods for modifying the surface layer include applying various protective wear-resistant coatings [1–3]. Another group includes methods of exposing the material surface to concentrated energy flows such as laser radiation [4, 5–8], electrons, or plasma, which lead to structural transformations in the near-surface layer and significantly stimulate atomic diffusion.

WC-Co based alloys are among the most important tool materials widely used for metal cutting. To vary the hardness and plasticity of these alloys, the cobalt concentration is usually changed, and carbides of titanium, tantalum, and other elements are added during synthesis. The effect of concentrated energy flows also changes the surface properties, for example, due to changes in the cobalt concentration in the surface layer caused by laser radiation [9] or due to structural and phase transformations that occur as a result of intense electron beam exposure [10].

Combined treatment of tools is now becoming increasingly common [11]. It involves the sequential use of two or more surface methods to obtain a composite with a complex set of properties that cannot be achieved by applying any of these methods alone. An example is the combined treatment of high-speed steel using the "Ritm-SP" installation. This installation is a source of low-energy intense electron beams combined with two magnetron sputtering systems placed in a vacuum chamber. It provides the deposition of films from various materials onto the product surface followed by liquid-phase mixing of the film and substrate materials with an intense pulsed electron beam [12], as well as the application of wear-resistant coatings by vacuum arc [13, 14].

The characteristics of this composite depend on the properties of both the coating and the modified layer. Many studies have focused on wear-resistant coatings, while the structure and properties of the interlayers remain poorly understood. This work presents the results of a study on the effect of irradiation with short (about  $5 \mu s$ ) pulses of low-energy electron beams on the

Impact factor: 2019: 4.679 2020: 5.015 2021: 5.436, 2022: 5.242, 2023:

6.995, 2024 7.75

structure, phase composition, and hardness of the near-surface layer of high-speed steel R6M5. This alloy was chosen because it has one of the simplest chemical compositions.

Based on the study of the structure of the modified subsurface layer, the conditions for the combined treatment of disk cutters were chosen. These cutters were made from uncoated high-speed steel R6M5, recommended by the manufacturer for processing heat-resistant chromium 34XH1MA alloys. To bind the free carbon that appears when tungsten carbide is irradiated by short pulses of low-energy electron beams, carbide-forming elements such as Nb and Hf were used; they have a higher affinity for carbon than tungsten and form stable carbide phases. These elements form carbides that can be eutectic or primary. These carbides have a high hardness of approximately 2400 HV, which exceeds the hardness of WC (about 1500 HV); however, tungsten carbide has even greater hardness at elevated temperatures. At high temperatures, niobium and hafnium carbides appear first directly in the melt. However, due to the high cooling rate of the melt, they do not have time to grow in the final product and remain small and evenly distributed. This should contribute to increased wear resistance and tensile strength.

The choice of alloy is also based on the fact that W-Hf-C alloys have high tensile strength [15]. The R6M5 alloy was irradiated in its initial state and after magnetron deposition of a Nb70Hf22Ti8 alloy layer with a thickness of 2-3  $\mu$ m to modify the surface.

Experimental Part. Samples of high-speed steel R6M5 had the shape of disk cutters and were ground to a surface roughness of Ra=0.03–0.06  $\mu$ m. These samples underwent: nitriding on the APP-2 installation, alloying on the "Ritm-SP" installation, and coating (TiAl)N on the Platit  $\pi 311$  installation. After magnetron deposition of the Nb70Hf22Ti8 alloy coating, some samples were irradiated in their initial state, and others were irradiated several times (the number of irradiations corresponds to the number of processing series). The processing conditions were chosen to simulate the thermal effect of the subsequent application of a wear-resistant coating by ion-plasma electric arc during combined surface treatment. Some samples were then tempered in a vacuum at 490°C for 1.5 hours (furnace cooling).

After surface alloying under optimal conditions, a gradient wear-resistant (TiAl)N coating with a thickness of 4  $\mu$ m was applied to the disk cutters for durability tests using the Platit  $\pi 311$  installation. The gradient coating structure starts with an adhesive TiN layer forming the coating base. The concentration of the AlN component monotonically increases toward the surface of the coating, increasing the coating microhardness up to 32 GPa. This coating has proven to be versatile and highly effective for finishing and rough machining under stable cutting conditions.

The phase composition and lattice parameters of the modified material layers were studied on a DronUM diffractometer with Bragg-Brentano focusing; in this case, the penetration depth of X-rays into the sample is an increasing function of the diffraction angle. The X-ray scan range was  $10.0-115.0^{\circ}$  with a step of  $0.1^{\circ}$ , and an exposure time of 4 seconds per point. However, these spectra are difficult to process because at high diffraction angles, the contribution from deeper sample layers is greater than at low angles. To exclude this effect from calculations, almost all measurements were conducted using asymmetric geometry, where the angle of incidence of X-rays on the sample was constant (in our case,  $10^{\circ}$ ).

Table 1. Conditions for NbHfTi Coating Deposition and Irradiation with Low-Energy Electron Beams.

Impact factor: 2019: 4.679 2020: 5.015 2021: 5.436, 2022: 5.242, 2023:

6.995, 2024 7.75

No	Deposition Parameter	Condition	Condition 2			
	NbHfTi Coating					
1	Magnetron power, W	350	350			
2	Argon pressure in the working chamber, mm Hg	$4.5 \times 10^{-3}$	$4.5 \times 10^{-3}$			
3	Thickness of the coating deposited by magnetron, µm	0.2	0.3			
	Irradiation					
1	Energy density in a single pulse, J/cm <sup>2</sup>	4.3	4.7			
2	Number of pulses	5	10			
3	Pulse duration, µs	5	5			
4	Pressure in the working chamber, mm Hg	$1.1 \times 10^{-3}$	$1.1 \times 10^{-3}$			
5	Number of treatment cycles	2	3			
6	Approximate thickness of the alloyed layer, µm	0.64	0.79			

The diffraction angle changes only due to the displacement of the detector. However, it should be noted that using such a geometry somewhat degrades the quality of the diffraction pattern, which manifests as increased peak broadening and decreased measured intensity. The calculations are based precisely on this spectrum, and apparently, the obtained substrate contribution, i.e., the bulk volume fraction of WC, indirectly indicates the thickness and continuity of the modified layer.

During the X-ray imaging, a copper anode X-ray tube was used. In this case, the depth of the layer contributing to the diffraction pattern formation is about 10  $\mu m$ . The concentration of alloying elements in the near-surface layer of the high-speed steel was estimated based on the nominal thickness of the alloyed layer, assuming that the alloy is not mixed within a layer approximately 5  $\mu m$  thick but rather represents a coating on the sample surface.

The wear resistance of the disk cutters was determined on a diagnostic stand based on the Jesco Machinery 1650ENC milling machine, equipped with an Fagor 800TGI NC controller and a three-component dynamometer 9257BA (Kistler Co.). The USB3000 device (R Technology Co.) was used as a universal data acquisition device. Experiments were carried out during axial turning of a cylindrical billet made from the heat-resistant alloy 34XH1MA under the following conditions: cutting speed v = 150 m/min, feed rate s = 0.10 mm/rev, and cutting depth t = 3 mm. Changes in total cutting force and wear of the tool's flank surface during machining were taken as criteria for evaluating the cutter's wear resistance. In practice, the service life of a metal-cutting tool is determined by flank wear. However, this criterion is not always objective because wear behavior may vary depending on machining conditions. Experimental results show that cutting force often provides a more objective criterion for the service life of disk cutters.

Results and Discussion

Impact factor: 2019: 4.679 2020: 5.015 2021: 5.436, 2022: 5.242, 2023:

6.995, 2024 7.75

The diffractogram of the initial sample shows peaks corresponding to WC carbide and  $\beta$ -Co. The cobalt concentration in the surface layer is lower than in the nominal composition and is about 1.5%. This may be related to cobalt loss during grinding.

After treatment of the P6M5 alloy with short pulses of low-energy electron beams (nine pulses with an energy density of 4.3 J/cm²), a network of cracks appears on the melted surface. However, the cracks are still small and can only be clearly seen at  $1000\times$  magnification. The block size of the crack network is about  $10~\mu m$ , comparable to the grain size of WC in the P6M5 high-speed steel (1–8  $\mu m$ ).

The diffractograms show new peaks corresponding to W2C carbides with an HCP lattice and, most likely,  $\gamma$ -WC with an FCC lattice (this phase is labeled as (W, Ti)C, although Ti is not present in the alloy), formed due to the extremely high cooling rates of the melt.

With more intensive irradiation (30 pulses with an energy density of 4.7 J/cm<sup>2</sup>), a distinct crack network with block sizes of 10– $20~\mu m$  appears on the insert surface. Peaks corresponding to  $\gamma$ -WC reflections noticeably broaden. It can be noted that the lattice parameter of the  $\gamma$ -phase WC changes from 4.248 to 4.274.

A weak reflex appears near  $2\theta \approx 26^{\circ}$ , likely corresponding to graphite, which results from carbide decomposition (see Tables 2 and 3).

After annealing at 490°C for 1.5 hours, a reflection near  $2\theta = 35^{\circ}$  appears in the diffractogram; this reflection may be associated with the formation of another carbide due to the partial decomposition of a metastable phase.

Table 2. Phase composition of the surface of the P6M5 cutter treated with nine pulses of a low-energy high-current electron beam with energy density 4.3 J/cm<sup>2</sup>.

If you want, I can also help translate the tables or any other part!

Фаза	Структурный	Объемная	Массовая	Периоды
	тип	доля,%	доля,%	решетки, Å
WC	hP3/2	$61.7 \pm 0.0$	$62.8 \pm 0.0$	A=2.900, C=2.833
γ-WC	cF8/2	$34.6 \pm 0.0$	$33.1 \pm 0.0$	A = 4.230
W <sub>2</sub> C	hP4/6	$3.7 \pm 0.0$	$4.2 \pm 0.0$	-

Unfortunately, we were unable to identify its structure (Table 4). After irradiation, the roughness of the insert practically does not change and remains at  $Ra = 0.05-0.07 \mu m$ . However, variations in microhardness were measured. The microhardness HV25 of the surface layer of the initial sample was 1150-1300, but for the irradiated sample, it decreased to 950-1100 regardless of the treatment conditions.

Table 3. Phase composition of the surface of the R6M5 milling cutter treated with nine pulses of a low-energy high-current electron beam with an energy of 4.3 J/cm<sup>2</sup>.

Phase	Structural type	Volume fraction, %	Mass fraction,	Lattice parameters, Å
WC	hP3/2	$5.6 \pm 0.0$	$7.6 \pm 0.0$	A=2.910, C=2.842
γ-WC	cF8/2	$93.5 \pm 0.1$	$91.0 \pm 0.1$	A = 4.248-4.274
$W_2C$	hP4/6	$0.9 \pm 0.0$	$1.4\pm0.0$	-

Impact factor: 2019: 4.679 2020: 5.015 2021: 5.436, 2022: 5.242, 2023:

6.995, 2024 7.75

Table 4. Phase composition of the surface of the R6M5 milling cutter treated with fifteen pulses of a low-current high-current electron beam with an energy of 4.7 J/cm<sup>2</sup> and annealed at 490°C for 1.5 hours.

Phase	Structural type	Volume fraction, %	Mass fraction,	Lattice parameters,
				Å
WC	hP3/2	$8.8 \pm 0.0$	$9.6 \pm 0.0$	A=2.904, C=2.836
γ-WC	cF8/2	$84.8 \pm 0.1$	$87.1 \pm 0.0$	A = 4.245
Карбид	cF8/2	$5.7 \pm 0.1$	$2.5 \pm 0.0$	4.470
W <sub>2</sub> C	hP4/6	$0.7 \pm 0.0$	$0.9 \pm 0.0$	-

This fact may also be related to the transformation of the surface structure and the precipitation of graphite. Surface modification of the high-speed tool steel R6M5 alloy with NbHfTi leads to the formation of a carbide designated as (Nb, Ti)C (niobium and hafnium are mutually infinitely soluble). Reflections of the  $\gamma\text{-WC}$  phase with a lattice period of 4.24 Å are clearly visible. Tables 5 and 6 present the corresponding diffraction patterns and surface microstructures. After alloying, the surface microstructure of the R6M5 insert significantly transforms, becoming finer and in some areas resembling a eutectic. Under processing conditions 1 (Table 1), no cracks appear on the surface, and surface roughness increases to Ra = 0.08–0.10  $\mu\text{m}$ . Under processing conditions 2 (Table 2), the surface still cracks, and surface roughness increases to Ra = 0.11–0.13  $\mu\text{m}$ . The cracking pattern differs from that occurring during processing without alloying: both fine and wide cracks are observed. No cellular crack structure was detected. Apparently, the applied power is currently too high for this alloying method.

Table 5. Phase composition of the surface of the R6M5 milling cutter alloyed by low-energy high-current electron beam treatment under conditions 1.

Phase	Structural type	Volume fraction, %	Mass fraction,	Lattice parameters, Å
WC	hP3/2	$20.4 \pm 0.1$	$30.1 \pm 0.1$	A = 2.895, C =
				2.832
γ-WC	cF8/2	$17.0 \pm 0.1$	$23.5 \pm 0.1$	A = 4.233
(Nb,Ti)C	cF8/2	$54.3 \pm 0.2$	$32.9 \pm 0.2$	A = 4.375
$W_2C$	hP4/6	$8.2 \pm 0.1$	$13.5 \pm 0.1$	A = 2.989, C =
				4.696

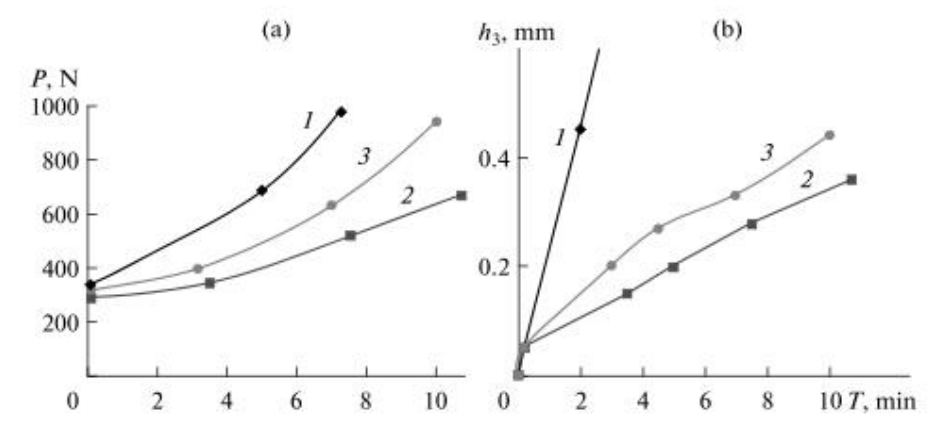
Table 6. Phase composition of the surface of the R6M5 milling cutter alloyed by low-energy high-current electron beam treatment under conditions 2.

mgn carrent electron count treatment under conditions 2.				
Phase	Structural	Volume fraction, %	Mass fraction,	Lattice parameters,
	type			Å
WC	hP3/2	$2.6 \pm 0.0$	$4.9 \pm 0.0$	A = 2.908, C = 2.844
γ-WC	cF8/2	$15.5 \pm 0.1$	$26.7 \pm 0.2$	A = 4.287
(Nb,Ti)C	cF8/2	$79.6 \pm 0.2$	$63.5 \pm 0.2$	A = 4.352
$W_2C$	hP4/6	$2.3 \pm 0.0$	$4.8 \pm 0.1$	A = 2.977, C = 4.623

Impact factor: 2019: 4.679 2020: 5.015 2021: 5.436, 2022: 5.242, 2023:

6.995, 2024 7.75

The surface microhardness increases to 1250–1350 HV25 under processing conditions 1 and to 1400–1650 HV25 under processing conditions 2. A comparison of the spectra recorded in symmetrical and asymmetrical configurations showed a change in the intensity of reflections of the two main cubic phases, which is associated with the presence of the {100} crystallographic



texture.

Fig. 1. Variations of (a) the total cutting force during milling and (b) the wear of the tool's flank face: (1) untreated; (2) combined treatment; (3) tool with coating.

Parallel to the sample surface; this texture is the result of directed heat removal during solidification of the molten surface. Therefore, it is quite difficult to estimate the fraction of niobium-hafnium-titanium carbides and  $\gamma$ -WC, although the amount of the (Nb, Hf, Ti)C phase on the surface is significantly greater than that of these carbides.

It is obvious that Nb, Hf, and Ti actively bind carbon. No reflections of graphite were observed. The W2C phase is clearly visible only in asymmetrical diffraction geometry, i.e., this phase apparently resides on the very surface of the sample. Annealing the modified alloy at 490°C does not lead to any structural transformations visible in the diffraction pattern, but the half-width of the diffraction lines slightly decreases, which may be related to the relaxation of internal stresses. Nevertheless, after annealing, there is a significant increase in surface microhardness. Regardless of the processing conditions, microhardness HV25 increases to 1950–2150. Apparently, a fine-dispersed phase precipitates; unfortunately, we were unable to identify this phase. However, literature discusses the possibility of dispersion strengthening in W-Hf-C alloys containing hafnium carbide or complex carbides (NbHfMo)CX as strengthening phases.

Based on the results of service life tests of disk cutters, it can be concluded that the increase in their service life after combined treatment, which includes alloying using low-energy high-current electron beams followed by coating application ((TiAl)N), reaches up to 100% (compared to untreated disk cutters) and up to 75% (compared to treated cutters) (Fig. 1a). The increase in service life, estimated by wear of the tool's flank face, is about 400–500% compared to untreated cutters and up to 40% compared to cutters with only wear-resistant coating (Fig. 1b).

#### **Conclusions**

This paper presents that the formation of the structure in the near-surface layer of the material is largely determined by the pulsed nature of the influence in the microsecond range. The key factors in the surface alloying process are the electron beam energy, dependent on the



Impact factor: 2019: 4.679 2020: 5.015 2021: 5.436, 2022: 5.242, 2023:

6.995, 2024 7.75

accelerating voltage, and the thickness of the thin film applied to the workpiece surface. The dependence of the modified layer thickness on the accelerating voltage has a pronounced extremal character. Irradiation with insufficient energy in the beam cannot initiate the process, while excessive energy leads to evaporation of most of the film. Treatment should be carried out so that the coating thickness is approximately half the depth of electron penetration into the substrate material, i.e., in our case about 200 nm.

The WC phase with a face-centered cubic lattice is present on the surface. In this case, graphite precipitates from the surface layer, which contributes to a decrease in surface microhardness by 200 HV25 compared to the original disk cutter (1150–1300 HV25), negatively affecting tool durability. It was established that micro-alloying the surface of high-speed steel R6M5 tools with Nb70Hf22Ti8 alloy contributes to the formation of a composition consisting of carbides WC,  $\gamma$ -WC, W2C, and (NbHfTi)C. This composition prevents graphite precipitation and positively affects surface microhardness, increasing it to 1400–1650 HV25.

When applying a protective wear-resistant coating, the tools were subjected to a temperature of 490°C for at least 1.5 hours. Modeling this effect showed an increase in surface microhardness to 1950–2150 HV25, which may be the result of dispersion strengthening of the micro-alloyed layer.

Service life test results showed that combined treatment increases the tool's failure-free service life by 1.5 times and reduces the overall cutting force; flank wear does not exceed 0.35  $\mu$ m. The increase in disk cutter service life, assessed by cutting force criteria and flank wear, indicates the promise of such combined treatment of high-speed tools.

#### References:

- 1. S.N. Grigoriev, Yu. A. Melnik, A.S. Metel, M.A. Volosova, Focused beams of fast neutral atoms in glow discharge plasma editors-pick, J. Appl. Phys. 121 (2017) 223302
- 2. S.N. Grigoriev, T.V. Tarasova, Possibilities of the technology of additive production for making complex-shape parts and depositing functional coatings from metallic powders, Metal Sci Heat Treatment 57 (2016) 579–584
- 3. S.N. Grigoriev, Study of cutting properties and wear pattern of carbide tools with comprehensive chemical-thermal treatment and nano-structured/gradient wear-resistant coatings, Mech. & Ind. 17 (2016) 702
- 4. Ж.О.Шарипов, С.У.Саидов, С.В.Фёдоров, Повышение стойкости поверхности зубцов дисковых фрез методом комплексной обработки. Науч. журнал Инженерные решения. № 5 (15), май, 2020 г.
- 5. Fedorov Sergey, Sharipov Jamshid, Odinaev Rustam, Sayliev Ismat, Saidov Sunnat, Mukhammadov Mukhsin, Improving the Surface Stability of the Teeth of Disk Cutters by Complex Processing. International Journal of Advanced Research in Science, Engineering and Technology. Vol. 7, Issue 5, May 2020
- 6. S.N. Grigoriev, S.V. Fedorov, M.D. Pavlov et al. Complex surface modification of carbide tool by Nb+Hf+Ti alloying followed by hardfacing (Ti+Al)N, J. Frict. Wear 34 (2013) 14–18
- 7. S.N. Grigoriev, Study of cutting properties and wear pattern of carbide tools with comprehensive chemical-thermal treatment and nano-structured/gradient wear-resistant coatings, Mech. & Ind. 17 (2016) 702

Impact factor: 2019: 4.679 2020: 5.015 2021: 5.436, 2022: 5.242, 2023: 6.995, 2024 7.75

- 8. S.V. Fedorov, M.D. Pavlov, A.A. Okunkova, Effect of structural and phase transformations in alloyed subsurface layer of hard-alloy tools on their wear resistance during cutting of high-temperature alloys, J. Frict. Wear Vol. 34 (2013) 190 198
- 9. A.S. Vereshchaka, Operability increase of edge cutters based on the directed modification of properties their operation surfaces at plating nano-structured multi-level composite coatings / A.S. Vereshchaka, S.N. Grigoriev, A.A. Vereshchaka, D.N. Lytkin, G.Yu. Savushkin, A.S. Suvenkov // Bulletin of MSTU "Stankin". 2014. No 4(31). pp. 45-51.
- 10. A.A. Vereshchaka, *Cutters with Modificating Antiwear Complexes*/ A.A. Vereshchaka, A.S Vereshchaka, M.I. Sedykh.— M.: MSTU "Stankin", 2014.—pp. 195.
- 11. A.A. Verashchaka, Effectiveness increase in functional coatings for cutters precipitable by KIB-MeVVA method through filtration steam-ionic flow for macro- and micro-particle separation/Verechaka A.A.—*Bulletin of MSTU "Stankin"*.—2015.—No 1(32).—pp. 41-48.
- 12. V.P.Tabakov, Methodological approaches to formation of cutter multi-level coatings / V.P. Tabakov, A.S. Vereshchaka, A.D. Batako // *Bulletin of Mechanical Engineering.*—2015.—No 9—pp. 82-88.
- 13. A.A. Vereshchaka, Edge ceramic tool with nano-structured multi-level composite coatings for highly rigid hardened steel finishing as alternative to finishing grinding / A.A. Vereshchaka, A.D. Batako, E.S. Sotova, A.S. Vereshchaka // Metal Science and Metal Thermal Treatment.—2015.— No 10 (724).—pp. 39-44.
- 14. S.V. Fedorov, A.A. Okunkova, N.Y. Peretyagin, P.Y. Peretyagin, Electroconductive graphene-hydroxyapatite PVD targets for magnetron sputtering, Izv. vyshih uchebnyh zaved. Fiz. 59 (2016) 192 194.
- 15. S.N. Grigoriev, S.V. Fedorov, Tool material surface alloying by wide-aperture low-energy high-current electron beam treatment before wear-resistant coating, Mech. & Ind. 16. (2015) 708